Volume 17
Number 18
14 May 2025
Pages 11085-11764

Nanoscale

rsc.li/nanoscale

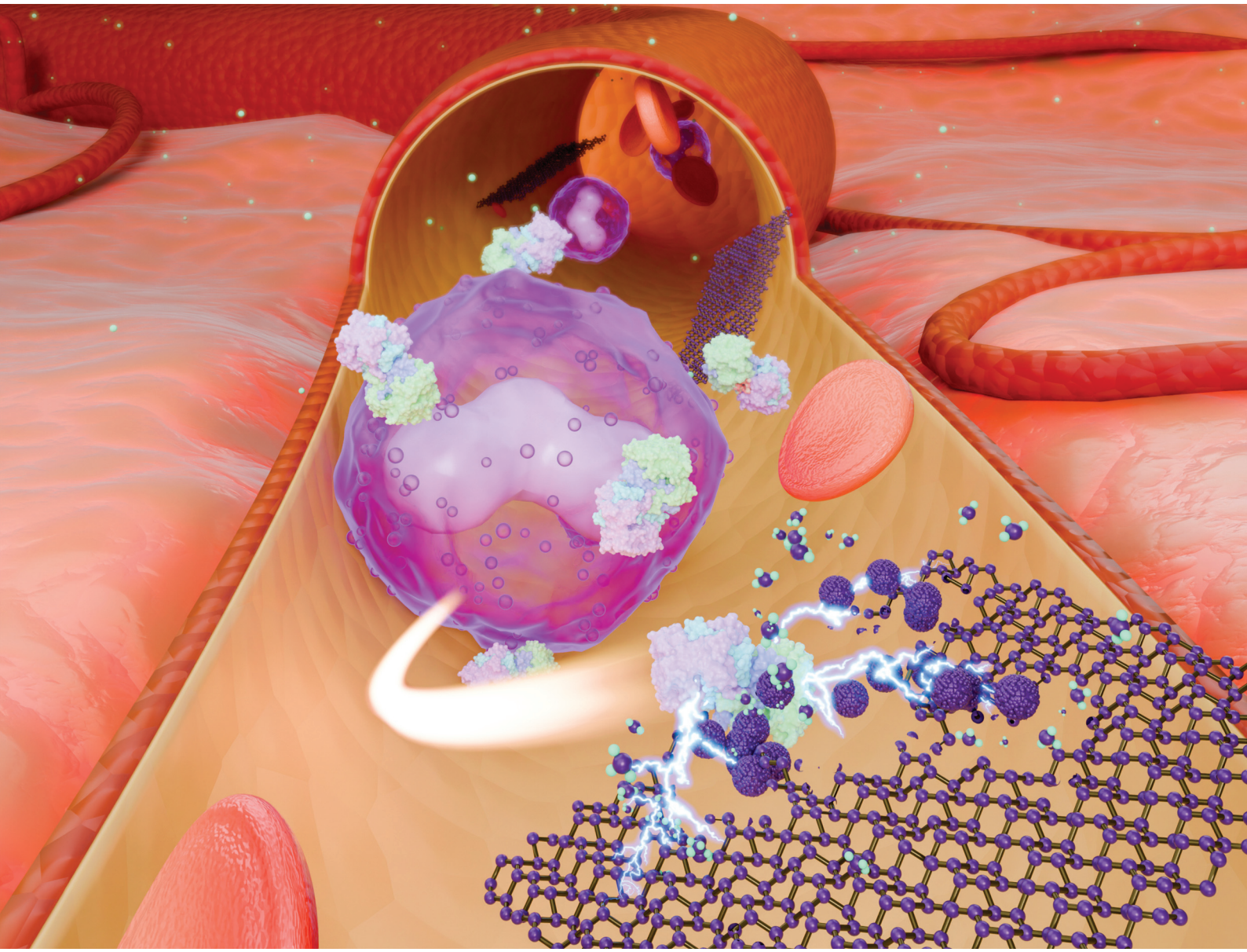

ISSN 2040-3372

ROYAL SOCIETY OF CHEMISTRY

COMMUNICATION

Carlo Altucci, Rajendra Kurapati *et al.*
Functionalization dependent biodegradability of two-dimensional antimonene by peroxidases: impact on immune modulation

NCNST

Nanoscale

COMMUNICATION

View Article Online
View Journal | View Issue

Check for updates

Cite this: *Nanoscale*, 2025, **17**, 11293

Received 14th November 2024,
Accepted 11th March 2025

DOI: 10.1039/d4nr04786a

rsc.li/nanoscale

Functionalization dependent biodegradability of two-dimensional antimonene by peroxidases: impact on immune modulation†

Jasneet Kaur,‡[a] K. Swetha, ‡[b] Manjot Singh, [c] Avazbek Abduvakhidov,[d] Michela Varra,[d] Manikrishna Lakavathu,[b] Jaber Adam,[c] Anjali Prajapati,[e,f] Srinivasa Reddy Bonam,[e,f] Carlo Altucci *[c,g] and Rajendra Kurapati *[b]

Antimonene (Sb) is an emerging two-dimensional material belonging to group VA that has shown excellent chemical and physical properties with applications in optoelectronics, energy, catalysis, and biomedical sciences. However, the biodegradability of Sb sheets in response to immune stimulation and its impact on degradation by-products have yet to be reported. Herein, we investigated the biodegradability of Sb nanosheets by treating them with human myeloperoxidase (hMPO) and plant peroxidase (horseradish peroxidase-HRP) in the presence of a low concentration of hydrogen peroxide. Furthermore, we studied the impact of non-covalently functionalized Sb nanosheets with 2-hydroxypropyl-β-cyclodextrin (Sb-CD) on their biodegradability. The biodegradability of Sb sheets was assessed using Raman spectroscopy, UV-vis spectroscopy and transmission electron microscopy. The results revealed that functionalized Sb sheets exhibited reduced degradability upon treatment with peroxidase due to the surface coating of β-CDs on Sb sheets. Next, the cytotoxicity results revealed that the pristine and functionalized Sb sheets and their by-degradation products did not affect human THP1 cells. Finally, the immune modulation studies with THP1 cells confirmed that Sb-nanosheets before and after partial degradation did not show significant production of TNF-α, confirming that Sb-nanosheets or degraded products played no role in the activation of the immune response. These results could provide better insights into the biodegradability of Sb sheets and their potential biomedical applications.

1. Introduction

Two-dimensional materials (2DMs) are highly attractive for various applications such as optoelectronics, energy, catalysis, and biomedical applications due to their unique chemical and physical properties.[1–5] Recently, an inorganic layered material, antimonene (Sb), was exfoliated using liquid-phase or mechanical exfoliation methods and exhibited excellent thermal conductivity and carrier mobility, along with spintronic properties.[6–8] Importantly, Sb materials are also being studied for potential biomedical applications such as NIR-photothermal applications for cancer theranostics,[9–11] drug delivery,[12] bioimaging,[13] *etc*. Interestingly, antimonial drugs are already used in clinical applications,[14] which indicates that Sb-based materials could be excellent candidates for nanomedicine applications over other 2D materials such as graphene, MoS_2, BP, *etc*. However, 2D Sb sheets are known to undergo surface oxidation under ambient conditions to form Sb_2O_3.[7,15] Furthermore, understanding the biodegradability of such potential 2D Sb sheets is essential to assess their *in vivo* fate and the long-term impact of degradation products on human health. The immune response to such 2D materials is found to be one of the important routes to understanding issues related to their biodegradability, including graphene family materials (GFMs) and other inorganic 2DMs. This can be done by directly incubating 2DMs with activated immune cells (neutrophils, macrophages, *etc*.) or treating them with peroxidase enzymes secreted by primary immune cells (neutrophils).[16–19] Such biodegradability of 2DMs has been reported for graphene family materials and inorganic 2DMs such as MoS_2, h-BN, MXenes, *etc*.[19,20]

However, the biodegradability of 2D Sb nanosheets by the action of peroxidase enzymes (human myeloperoxidase-hMPO)

[a]*Dept of Physics "Ettore Pancini", Università degli Studi di Napoli "Federico II", via Cintia 21 – Building 6, 80126 Napoli, Italy*
[b]*School of Chemistry, Indian Institute of Science Education and Research Thiruvananthapuram, Maruthamala PO, Vithura 695551, Kerala, India. E-mail: rkurapati@iisertvm.ac.in*
[c]*Dept of Advanced Biomedical Science, Università degli Studi di Napoli "Federico II", via S. Pansini 5, 80131 Napoli, Italy. E-mail: carlo.altucci@na.infn.it*
[d]*Dept of Pharmacy, Università degli Studi di Napoli "Federico II", Via D. Montesano 49, 80131 Naples, Italy*
[e]*Vaccine Immunology Laboratory, Department of Applied Biology, CSIR-Indian Institute of Chemical Technology, Hyderabad 500007, Telangana, India*
[f]*Academy of Scientific and Innovative Research, Ghaziabad 201002, India*
[g]*Istituto Nazionale Fisica Nucleare (INFN), via Cintia 21 – Building 6, 80126 Napoli, Italy*

†Electronic supplementary information (ESI) available. See DOI: https://doi.org/10.1039/d4nr04786a

‡Equal contribution.

Open Access Article. Published on 25 marca 2025. Downloaded on 02.02.2026 17:35:17.
This article is licensed under a Creative Commons Attribution-NonCommercial 3.0 Unported Licence.

Open Access Article. Published on 25 marca 2025. Downloaded on 02.02.2026 17:35:17.
This article is licensed under a Creative Commons Attribution-NonCommercial 3.0 Unported Licence.

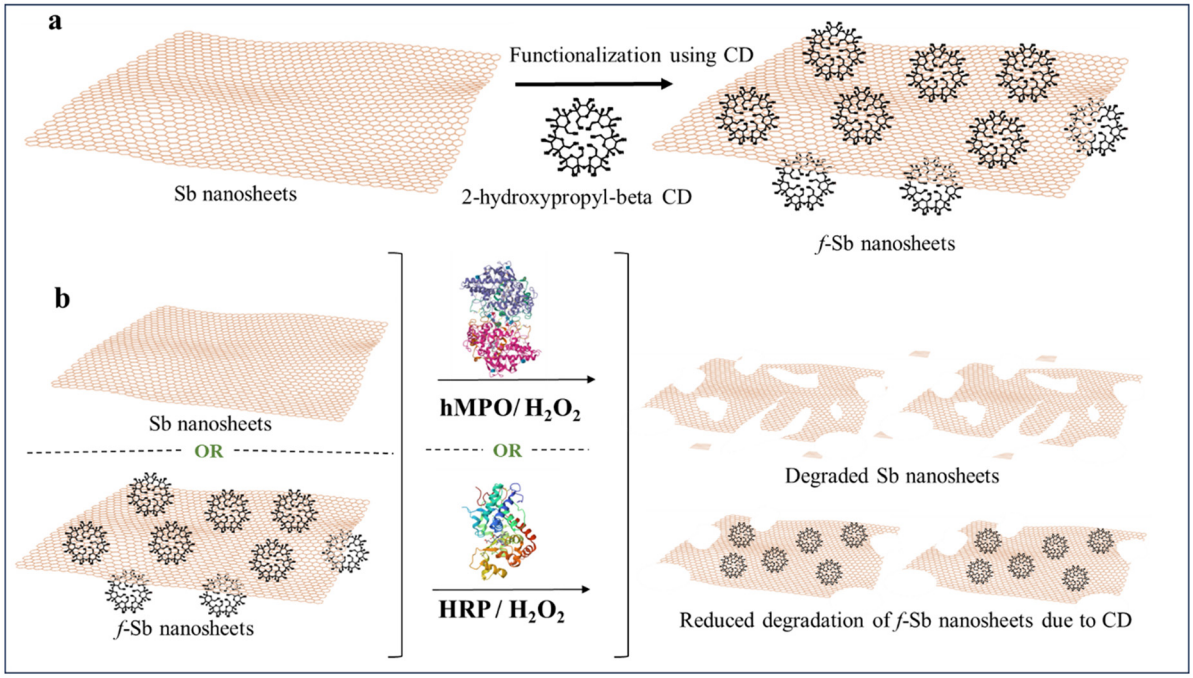

Scheme 1 (a) Functionalization of Sb nanosheets using 2-hydroxypropyl-β-cyclodextrin (β-CD) to obtain f-Sb nanosheets and (b) biodegradation of Sb and f-Sb nanosheets using the human enzyme hMPO and the plant enzyme HRP in low concentrations of hydrogen peroxide, respectively.

has yet to be reported. Herein, we report the biodegradability of pristine 2D Sb nanosheets and cyclodextrin functionalized nanosheets (f-Sb) by the enzymatic catalysis of hMPO and plant peroxidase (HRP) in the presence of H_2O_2 (Scheme 1). The degradation was investigated using spectroscopic and microscopic techniques. Also, the cytotoxicity of the Sb sheets, before and after degradation, was studied to understand the impact of these Sb materials and their degradation products on human cells.

Rajendra Kurapati

Rajendra Kurapati obtained a PhD from the Indian Institute of Science, Bangalore. Kurapati worked as a Post-Doc with Prof. Alberto Bianco at CNRS, University of Strasbourg (2014-17), investigating the biodegradation of 2D materials. In 2018, Kurapati received the Marie Skłodowska-Curie fellowship with Prof. Abhay Pandit at CÚRAM, the University of Galway, Ireland. In 2021, Kurapati received the prestigious DBT-Ramalingaswami Faculty fellowship at the University of Hyderabad, India. Since 2021, Kurapati has been an Assistant Professor of Chemistry at IISER Thiruvananthapuram. Kurapati's Biomaterials Lab is at the forefront of understanding the biodegradation of nanomaterials, microplastics, nano-immune cell interactions and development of Biomaterials for antimicrobial coatings, drug/gene delivery and sustainable bioplastic.

2. Materials and methods

Sb bulk powder and 2-hydroxypropyl-beta-cyclodextrin were purchased from Sigma-Aldrich. The enzyme human myeloperoxidase (hMPO, isolated from human polymorphonuclear leukocytes) and horseradish peroxidase (HRP) were commercially obtained from Sigma-Aldrich, India. The chemicals $Na_2HPO_4{\cdot}2H_2O$, $NaH_2PO_4{\cdot}2H_2O$, NaCl, KCl, KH_2PO_4, hydrogen peroxide (30% aqueous solution) and diethylenetriamine penta acetic acid (DTPA) were obtained from Sigma-Aldrich and used directly without any further purification. Deionized water (DI) was acquired using a Milli-Q® Millipore filter system.

2.1 Synthesis of Sb nanosheets

First, 100 mg of bulk Sb powder (initial concentration of 5 mg mL^{-1}) was dispersed in 20 mL of DI water. The dispersion was then exfoliated by combining probe and bath sonication processes.[21] During the probe sonication process, an ice bath was employed to prevent heat generation due to cavitation bubbles. After sonication, the dispersion was centrifuged at room temperature at 3000 rpm for 20 minutes to remove the unexfoliated Sb from the solution. Finally, the sediment part was discarded, and the supernatant was collected and stored at 4 °C for further use.

This journal is © The Royal Society of Chemistry 2025

Open Access Article. Published on 25 marca 2025. Downloaded on 02.02.2026 17:35:17.
This article is licensed under a Creative Commons Attribution-NonCommercial 3.0 Unported Licence.

2.2 Functionalization of Sb sheets with 2-hydroxypropyl-β-cyclodextrin

According to a previous report, Sb sheets were functionalized with 2-hydroxypropyl-beta-cyclodextrin (CD).[22] Briefly, 180 mg of CD (initial concentration, 9 mg mL^{-1}) and 100 mg of Sb bulk powder (initial concentration, 5 mg mL^{-1}) were dispersed in 20 mL of DI water. The resulting dispersion was exfoliated using probe and bath sonication, respectively. After sonication, the dispersion was centrifuged at 3000 rpm for 20 minutes, and the sediment was discarded. Finally, the supernatant was collected and stored at 4 °C for further characterisation.

2.3 Characterization of Sb and f-Sb nanosheets

2.3.1 Ultraviolet–visible spectroscopy. The ultraviolet-visible (UV) absorption spectra of Sb and f-Sb nanosheets were obtained using a spectrophotometer (Shimadzu UV-3600 Vis-NIR spectrophotometer). The analysis was then performed using a 1 mL quartz cuvette with a light path length of 10 mm. All the measurements were taken at room temperature and baseline correction was performed using water as a blank.

2.3.2 Zeta potential measurements. The size and surface charges of Sb and f-Sb nanosheets were measured using a Zetasizer Nano-ZS instrument (Malvern Instruments, Malvern, UK). The samples underwent 1 minute of sonication before the measurements. All the measurements were taken at room temperature using a disposable zeta sizer cuvette. Each measurement was repeated 3 times, and the results are presented as the mean and standard deviation.

2.3.3 Raman spectroscopy. Raman spectroscopy was employed to characterize the pristine Sb and f-Sb nanosheets using a LabRAM HR Raman spectrophotometer with a 633 nm laser at 3% power and using a microscope. Both samples were sonicated for 5 minutes. Then, 6 μL of each sample was drop-casted onto two separate clean glass slides and dried under IR radiation. Raman spectra were recorded using a 100× objective lens. The graphs were plotted using Origin software, where the baseline correction was done by subtracting the origin values, with 8 points selected in the graph. The Raman characterization of exfoliated (thin) sheets is very difficult because of very low non-resonant Raman intensities,[23] and therefore, we could not get more Raman spectra for each sample, unlike graphene materials. The Raman plots present only one spectrum.

2.3.4 Fourier transform infrared spectroscopy. Fourier transform infrared (FTIR) spectra of samples were collected using a Jasco FT/IR 4100 spectrometer (Easton, MD) in a single-reflection ATR with an ATR PRO ONE X (Jasco) equipped with a ZnSe prism (ATR/sample contact area of 2.5 mm diameter, no. of reflections = 1 and an angle of incidence of 45°) at a resolution of 2 cm^{-1} and a total of 100 scans (scan range 4000–550 cm^{-1}). Spectra were acquired in triplicate on three different samples of 2-hydroxypropyl-β-cyclodextrin and f-Sb nanosheets.

2.3.5 Transmission electron microscopy (TEM). The morphology and lateral dimension of the nanosheets were meticulously examined using transmission electron microscopy (TEM) (FEI TECHNAI G2 F30 S-Twin, operating at 120 kV). The sample was subjected to 5 minutes of sonication using an ANM Industries ultrasonic cleaner (USC-300 50 Hz). Nearly 10 μL of each sample was deposited on a carbon-coated copper TEM grid and left to dry for 20 minutes under an IR lamp.

2.3.6 X-ray photoelectron spectroscopy. Sb and f-Sb nanosheets underwent examination utilizing X-ray photoelectron spectroscopy (XPS) (Omicron Nanotechnology XPS) and the data acquisition was performed using VISION software, while data interpretation was performed using CASAXPS software (Casa Software Ltd, UK). The analysis was carried out with a monochromatic AL K X-ray source (1486.7 eV) operating at 15 kV (90 W).

2.4 Colloidal and chemical stability of Sb nanosheets with and without functionalization

In order to study the chemical stability of both types of nanosheets, 2 mL of each prepared nanosheet was taken in separate vials. The UV spectra of each vial were recorded daily over 4 days. The data were also recorded on the same day and the nanosheets were synthesized. All the measurements were recorded at room temperature and baseline correction was performed using water as a blank control.

2.5 Degradation of Sb and f-Sb nanosheets with the HRP enzyme

For the degradation with HRP, 78.33 μL of Sb nanosheets (final concentration of −0.3 mg mL^{-1}) was added to 921.67 μL of PBS buffer. For f-Sb nanosheets, 67 μL of nanosheets (final concentration of 0.6 mg mL^{-1}) was added to 933 μL. To both suspensions, 0.175 mg of HRP was added. 4 μL of 10 mM H_2O_2 were added daily for ten days. All suspensions were maintained under dark conditions and were subjected to continuous stirring throughout the experimental period. The portions of 20 μL were collected at 0, 5, and 10 days and stored at −20 °C for further characterization.

Similarly, sample degradation was conducted using the same amount in the absence of HRP. 4 μL of H_2O_2 was added once daily for 10 days.

2.6 Degradation of Sb and f-Sb nanosheets with the hMPO enzyme

Next, 42 μL of Sb nanosheet solution was added to 70.5 μL of 50 mM PBS buffer (final concentration is 0.3 mg mL^{-1}). To this suspension, 12.5 μL of hMPO (1 mg mL^{-1}), pre-dissolved in PBS buffer, was added. Every hour, 2 μL of 10 mM H_2O_2 was added for 10 hours. The hMPO enzyme was refreshed every 5 hours. The reaction mixture was kept at 37 °C in an incubator. The fractions of 10 μL were collected at 0 h, 5 h, and 10 h and stored at −20 °C until they were characterized using various techniques. To investigate the degradation process without hMPO, 42 μL of Sb nanosheets was combined with 70.5 μL of PBS buffer. Subsequently, 2 μL of H_2O_2 was added every hour for 10 hours.

Likewise, the degradation of f-Sb nanosheets was conducted by adding 12.5 μL of f-Sb nanosheets (final concentration:

Open Access Article. Published on 25 marca 2025. Downloaded on 02.02.2026 17:35:17.
This article is licensed under a Creative Commons Attribution-NonCommercial 3.0 Unported Licence.

0.9 mg mL^{-1}) to 98 μL of PBS buffer. 12.5 μL of hMPO was introduced. Next, 2 μL of H_2O_2 was introduced every hour for 10 hours. In the same way, the degradation only in the presence of H_2O_2 was carried out by adding 12.5 μL of f-Sb nanosheets to 99 μL of PBS buffer. The reaction was carried out at 37 °C.

2.7 Characterization of degraded Sb and f-Sb nanosheets

2.7.1 Raman analyses. Raman analyses were performed on the degraded samples (buffer and buffer/H_2O_2/enzyme) for both types of nanosheets (Sb and f-Sb) using a LabRAM HR Raman spectrophotometer equipped with a 633 nm laser at 3% power and a microscope. All the samples were sonicated for 5 minutes before deposition on clean glass slides. Next, 6 μL of each sample was drop-cast and dried under IR radiation. Raman spectra were recorded using a 100× objective lens.

2.7.2 Transmission electron microscopy analyses. TEM analyses were conducted using an FEI TECNAI G2 Spirit BioTwin microscope with an accelerating voltage of 120 kV. Next, 6 μL of each degraded sample (buffer, buffer/H_2O_2, and buffer/H_2O_2/enzyme) for both types of nanosheets (Sb and f-Sb) was drop-cast onto separate carbon-coated copper TEM grids. The grids were dried under an IR lamp for 20 minutes and then washed with Milli-Q water for approximately 8–10 minutes to remove salts from the buffer. Finally, the grids were again dried under an IR lamp for another 20 minutes.

2.8 Cell viability of Sb and f-Sb nanosheets before and after degradation

Cytotoxicity was assessed using a colorimetric assay based on the reduction of 3-[4,5-dimethylthiazol-2-yl]-2,5-diphenyl-tetrazolium bromide (MTT) by mitochondrial dehydrogenases in viable cells, resulting in the formation of a blue formazan precipitate.

2.8.1 THP-1 human monocyte cells. The cytotoxicity of the pristine Sb and f-Sb nanosheets before and after partial degradation was assessed on THP-1 cells. Partial degradation was performed by incubating pristine Sb and f-Sb nanosheets in PBS buffer for 3–4 days. THP-1 cells were maintained in complete RPMI-1640 medium (Sigma-R6504) supplemented with 10% fetal bovine serum (FBS) (Gibco-16170078) and 1% penicillin–streptomycin (Gibco-15140-122) solution under standard conditions of 37 °C and 5% CO_2 for 24 hours. THP-1 cells were added to a 96-well plate at a density of 10000 cells per well. Then, the cells were treated with decreasing concentrations of Sb and f-Sb nanosheets and partially degraded Sb and f-Sb nanosheets (1 μg ml^{-1}–20 μg ml^{-1}) and incubated for 24 hours at 37 °C and 5% CO_2. Before treatment, non-degraded, pristine and functionalised nanosheets were freshly reconstituted as per the concentrations. The experiment was conducted in triplicate for each concentration of each nanosheet. Control wells contained only the cells without any treatment. After 24 hours of incubation, 50 μL of MTT (Sigma, M5655) solution (5 mg mL^{-1} concentration in PBS) was added into each well and incubated for 4 hours at 37 °C and 5% CO_2 for 24 hours. Later, ~100 μL of media was aspirated and discarded, and formazan crystals were dissolved in 50 μL of dimethyl sulfoxide (DMSO) and incubated for 15 minutes. Absorbance (O.D.) was then measured at 570 nm using a MEGALLAN (Tecan Life Sciences) microplate reader. Percentage cell viability was then calculated based on the nanosheet treatment's absorbance relative to the cell control's absorbance.

2.9 Cytokine TNF-α production analysis: ELISA

Secreted cytokines were measured by sandwich enzyme-linked immunosorbent assay (ELISA). For this, human THP-1 monocytic cells (1×10^6 cells) were cultured in a 48-well tissue culture plate in a complete medium (RPMI-10% FBS). The cells were then treated with pristine Sb and f-Sb nanosheets before and after partial degradation with a concentration of 5 μg mL^{-1} and incubated at 37 °C with 5% CO_2 for 24 hours. Culture supernatants were then collected and centrifuged at 1500 rpm for 5 minutes to remove any cell debris. TNF-α in supernatants was measured using ELISA kits (Human TNF-α DuoSet ELISA kit, DY210-05) following the manufacturer's protocol.

2.10 Statistical analysis

Data were analysed using GraphPad Prism 8. A comparison of two groups was performed either using Student's unpaired and paired *t*-tests or with Mann–Whitney rank sum nonparametric and parametric tests depending on the results.

3. Results and discussion

3.1 Synthesis and characterization of Sb and f-Sb nanosheets

First, pristine Sb and CD functionalized f-**Sb** sheets were exfoliated using probe and bath sonication similar to the functionalization of β-CDs with 2D MoS_2 and ReS_2 sheets.[22] First, a broad peak at 250–260 nm in the UV-vis spectrum (Fig. 1a) of pristine Sb nanosheets indicates the formation of exfoliated Sb sheets.[24] Meanwhile, a small shift in the UV-vis peak of f-Sb sheets could be due to the stabilization of hydrophobic Sb sheets by the surface coating or adsorption of β-CDs containing hydrophilic functional groups similar to β-CD functionalized 2D MoS_2.[22] As β-CDs have minimal absorbance between 200 and 400 nm, the shift in f-Sb could be attributed to the surface adsorption of β-CDs on the Sb sheets. Furthermore, the pristine Sb nanosheets initially exhibited a surface potential of −25.6 ± 5.03 mV; however, upon functionalization with β-CDs, the negative potential of f-Sb shifted to −18.8 ± 3.67 mV, indicating the functionalization of Sb sheets, thereby reducing its aqueous oxidation (Fig. S1†).[25] Dynamic light scattering (DLS) revealed that the size of Sb sheets ranges from ~200 to 500 nm (Fig. S2†). Furthermore, Raman spectroscopy was employed to evaluate the formation of antimonene sheets (Fig. 1b and c).[26] The Raman spectra of pristine Sb sheets show fundamental peaks at 118 cm^{-1} and 149 cm^{-1} corresponding to the E_g (in-plane vibrations of Sb atoms) and $A^1{}_g$ vibration modes (out-of-plane vibrations per-

 This journal is © The Royal Society of Chemistry 2025

Open Access Article. Published on 25 marca 2025. Downloaded on 02.02.2026 17:35:17.
This article is licensed under a Creative Commons Attribution-NonCommercial 3.0 Unported Licence.

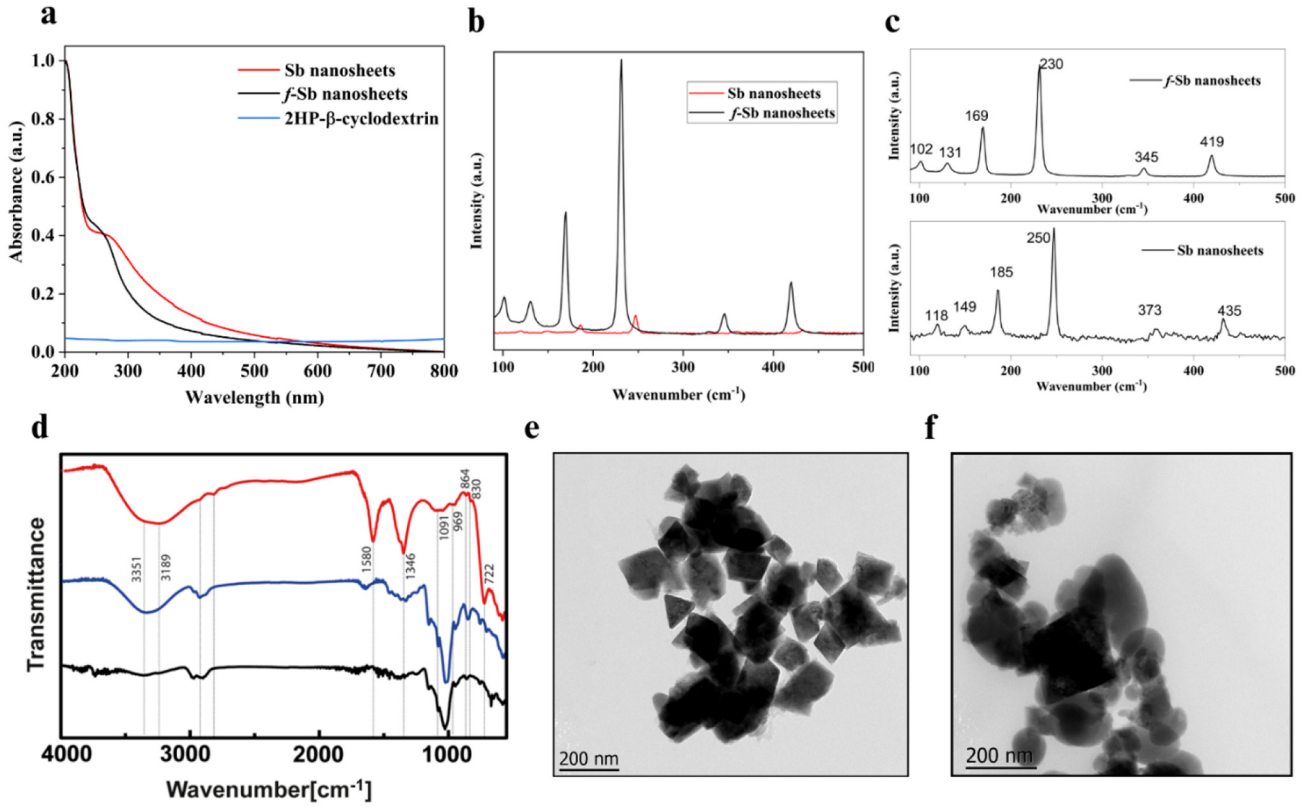

Fig. 1 Sb and f-Sb nanosheet synthesized by LPE. (a) UV-vis absorption spectra of pristine Sb (red line), f-Sb nanosheets (black line), and 2HP-β-cyclodextrin (blue line) in water, respectively, (b) Raman spectra of Sb nanosheets (red line) and f-Sb nanosheets (black line) exfoliated in water, respectively. (c) Raman spectra of Sb nanosheets (bottom) and f-Sb nanosheets (top) show distinctive peaks for each type of nanosheet vibration mode, respectively, (d) FTIR spectra of 2-HP-β-cyclodextrin (blue line), Sb nanosheets (red line) and f-Sb nanosheets (black line). HR-TEM images of (e) Sb nanosheets and (f) f-Sb nanosheets, respectively.

pendicular to the crystal lattice) of 2D Sb, respectively.[27,28] Furthermore, the intense peaks at 185, 250, 373 and 435 cm^{-1} indicate oxide forms of Sb due to aqueous oxidation.[29–31] In the case of f-Sb sheets, Raman spectra show all the peaks similar to pristine Sb; however, there is a shift towards a lower wavenumber and enhanced intensity, which could be due to the surface adsorption of β-CDs on the Sb sheets.[13]

To further confirm the binding between the Sb sheets and the β-CDs, FTIR spectra were analysed (Fig. 1d). For pristine Sb exfoliated in water (red line), the peaks at around 722 and 830 cm^{-1} were ascribed to Sb–O–Sb and Sb oxide vibrations in Sb_2O_3, whereas the two extensively overlapped bands in the range of 3600–2600 cm^{-1}, as well as those at ~1580 and 1346 cm^{-1}, could be due to the vibrational modes of strongly surface adsorbed water molecules.[32] These results suggested that by applying sonication in a water-based suspension, Sb underwent significant oxidation, at least on the surface of the sheets.[21,28] The FTIR spectrum of β-CDs (blue line) showed a characteristic, intense band at around 3300 cm^{-1} due to O–H stretching vibrations and two weak, partially overlapped bands at around 2900 cm^{-1} caused by asymmetric and symmetric C–H stretching vibrations.[33] These bands, in the FTIR spectrum of lyophilized f-Sb nanosheets (black line), showed a noticeable variation in their relative intensities, suggesting that the oxygen-containing functional groups of β-CDs could replace water molecules in the interaction with Sb nanosheets. Further differences in the FTIR spectra were also appreciable in the range of 600–1500 cm^{-1} (see Fig. S3,† for details). The overall data supported the involvement of oxygen-containing functional groups of β-CDs in the interaction with the Sb sheets. These interactions could involve the formation of hydrogen bonds between –OH on β-CDs and the oxygen atoms on the oxidized Sb nanosheet surface. Next, HR-TEM was employed to determine the morphology and size of both types of nanosheets. The HR-TEM images of the Sb nanosheets (Fig. 1e) illustrate the polydisperse nature of the Sb sheets, with sizes ranging from 200 to 500 nm. These results are consistent with DLS size analysis (Fig. S2†). Furthermore, the f-Sb nanosheets (Fig. 1f) functionalized with β-CDs exhibit a size range of 200–500 nm, aligning with the findings of DLS. Furthermore, XPS analyses (Fig. S5, S6 and Table S1†) depict the spectra of Sb nanosheets: the Sb 3d peaks can be deconvoluted into two components: Sb $3d_{3/2}$ and Sb $3d_{5/2}$, at 534 and 537 eV, which corresponds to the Sb_2O_3 oxidation states of antimonene. The peak at 532.2 eV corresponds to the O1s, indicating the presence of oxygen on the surface of Sb,[34]

Open Access Article. Published on 25 marca 2025. Downloaded on 02.02.2026 17:35:17.
This article is licensed under a Creative Commons Attribution-NonCommercial 3.0 Unported Licence.

thereby confirming that the surface of the sheets oxidized during preparation in the water. Additionally, longer sonication times further enhance this oxidation process, as evidenced by the increased intensity of the oxygen-related peaks in the XPS spectra.[35] Furthermore, Fig. S6b† illustrates the spectra for f-Sb, and the peak at 532.2 eV corresponds to the O1s, which has a lower intensity than that observed in the Sb nanosheets. This suggests that the surface was oxidized, although not to the same extent as the bare ones, as the β-CD molecules covered the surface of nanosheets through adsorption. This observation supports the conclusion that the Sb nanosheets are more prone to oxidation than the functionalized ones.

3.2 Chemical stability studies

Furthermore, monitoring the degradation of nanosheets in an aqueous environment is crucial for understanding their stability and potential environmental impact. The use of UV-vis spectroscopy is a common method to track these changes. This method provides a non-invasive way to study the nanosheet behaviour over time, offering insights into their longevity and the timing of their oxidation. Hence, UV-vis absorption measurements were conducted for Sb suspensions (Fig. 2). In the case of Sb nanosheets, the observed decrease in intensity over the initial two days could indeed be attributed to the precipitation or reaggregation phenomenon, which does not necessarily imply degradation.[36] It is also obvious that the dispersion of Sb NSs in pure water results in poorer stability as compared to the Sb NSs dispersed in organic solvents.[37] The sonication process in itself induces oxidation during the fabrication of Sb NSs due to the activation of high sonic jets and cavitation bubbles producing very high energy, enabling atmospheric oxygen to go inside the structure of Sb NSs, resulting in Sb_2O_3 or Sb_2O.[38] Prolonged dispersion over several days increases the surface oxidation layer and oxidation composition of the exfoliated material. In agreement with the literature, with an increase in the oxidation degree, as in our case, the lattice thermal conductivity of the material decreases, which, as a result, affects the physical properties of the material, decreasing the absorbance intensity of bare Sb NSs.[35,39] On the other hand, f-Sb NSs exhibit a less oxidized surface in comparison with bare Sb NSs. The slower decrease in the absorbance intensity of f-Sb NSs can be attributed to the slower degradation and less oxidation of the oxidized passivation layer of Sb NSs.[13,40] This substantially agrees with our XPS and FTIR results, confirming a high degree of oxidation for bare Sb compared to f-Sb-NSs.

3.3 Degradation of Sb and f-Sb nanosheets using hMPO

The biodegradation of both Sb and f-Sb nanosheets was studied using the peroxidase enzyme predominantly found in neutrophils and macrophages, known as hMPO enzyme. The study of biodegradation was significant in presenting intriguing insights into the fate of the nanosheets in humans and their potential biomedical applications. Briefly, pristine and f-Sb nanosheets were treated with hMPO dispersed in PBS buffer in the presence of H_2O_2, which was renewed per hour. The total hMPO treatment was performed for 10 hours. Next, the morphological and structural changes in the Sb sheets after degradation were characterized using TEM and Raman spectroscopy. First, TEM analyses of the control Sb and f-Sb nanosheets showed no significant morphological changes before (Fig. 3a and e) and after 10 h of incubation in PBS (Fig. 3b and f). However, there is a remarkable difference in the morphology of both Sb and f-Sb sheets after 10 h of incubation with hMPO/H_2O_2, which can be attributed to oxidation/degradation that resulted in the formation of debris and fragmented nanosheets. The Sb sheets lost their characteristic sheet morphology and found nanoscale debris or fragments compared to the control samples (Fig. 3d and h). Next, Sb and f-Sb nanosheets showed minimal damage or degradation after incubating in H_2O_2 alone without adding hMPO for 10 h (Fig. 3c and g). The results also confirm that f-Sb nanosheets underwent less degradation than the pristine Sb sheets, which could be attributed to the surface coating of the cyclodextrin molecules on the Sb sheets, thereby providing protection and stability to

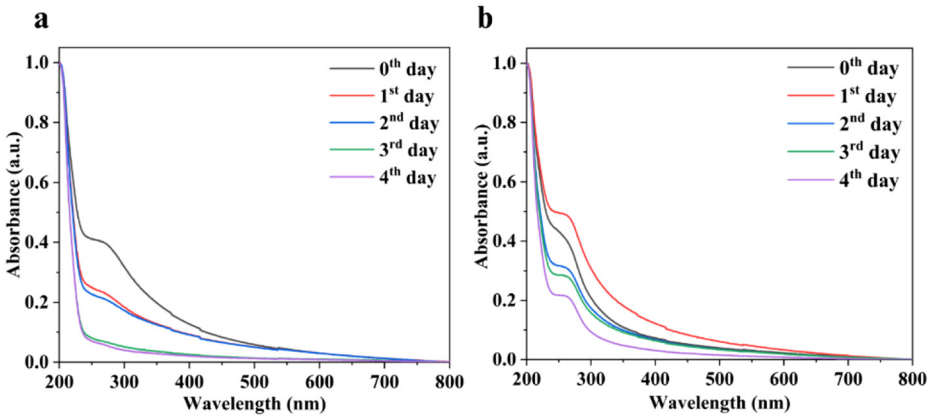

Fig. 2 Chemical stability studies of (a) Sb nanosheets and (b) f-Sb nanosheets over five days, characterized using UV-visible absorption spectroscopy, respectively.

 This journal is © The Royal Society of Chemistry 2025

Open Access Article. Published on 25 marca 2025. Downloaded on 02.02.2026 17:35:17.
This article is licensed under a Creative Commons Attribution-NonCommercial 3.0 Unported Licence.

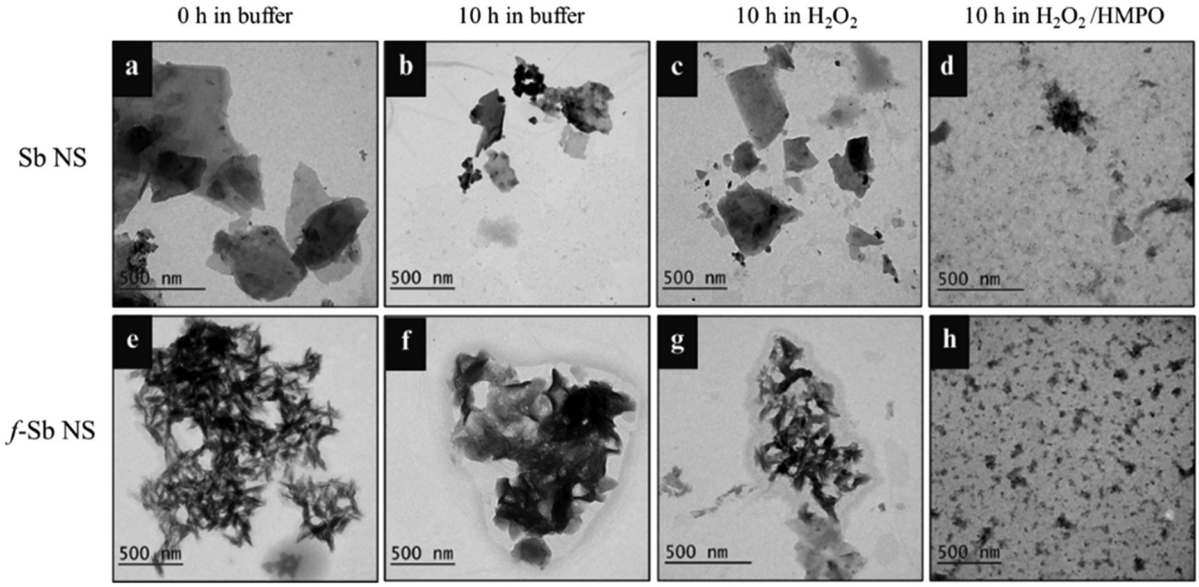

Fig. 3 TEM images of hMPO-catalysed degradation of (a) Sb NSs and (e) f-Sb NSs dispersed in buffer at 0 h, respectively. (b) Sb NSs and (f) f-Sb NSs after 10 h of incubation in the buffer. (c) Sb NSs and (g) f-Sb NSs in the buffer along with H_2O_2 after 10 h of incubation. (d) 10 h treated Sb NSs and (h) f-Sb NSs with PBS/H_2O_2/hMPO.

the nanosheets.[41,42] Similar results were also reported for other inorganic 2D materials, such as MoS_2, where chemical functionalization reduced the degradability of f-MoS_2 sheets over the pristine ones upon hMPO treatment.[19,43]

Furthermore, the samples were analysed using Raman spectroscopy to investigate the possible oxidation or degradation by hMPO. Fig. 4a shows the spectra of the nanosheets in buffer at 0 h and 10 h, respectively. At 0 h, all the main characteristic peaks of the Sb nanosheets were present; however, after 10 h, the intensity of those peaks was reduced, and peaks at 375 and 453 cm^{-1} were broadened, corresponding to the oxide form of the Sb sheets.[29–31] These results suggested that there were structural changes due to the gradual oxidation process affecting the Sb layers in the buffer alone. Next, the Raman spectra of the Sb nanosheets after degradation using hMPO/H_2O_2 showed no characteristic peaks of the Sb sheets, confirming the oxidation or degradation of Sb nanosheets. However, Raman spectra of f-Sb sheets (Fig. 4b) display all the characteristic peaks of Sb at 0 h in PBS, and those peak intensities subsequently reduced after 10 h of incubation in PBS, possibly due to mild oxidation of Sb sheets in the PBS alone.[29–31] Furthermore, in the presence of hMPO/H_2O_2, there were no characteristic peaks observed for Sb nanosheets, whereas a small broad peak at 456 cm^{-1} corresponding to the oxide form of Sb was observed.[29–31] This indicated that the sheets were partially degraded compared to the pristine Sb

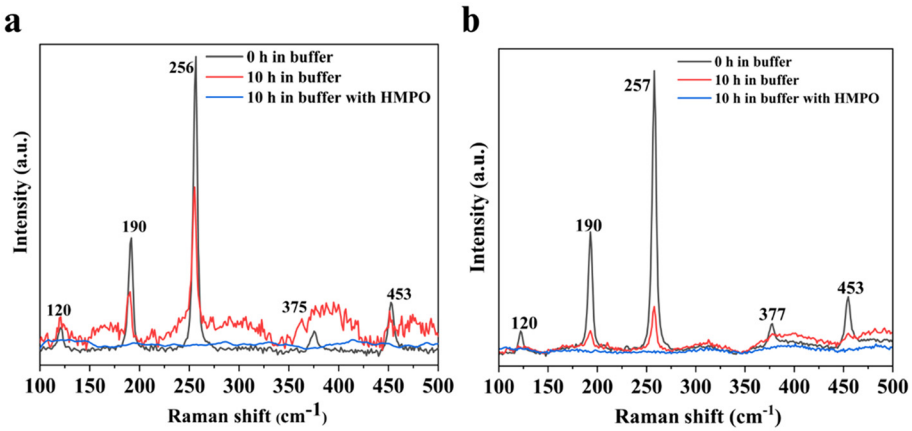

Fig. 4 Raman spectra of (a) Sb NSs dispersed in buffer at 0 h (black line), after 10 h of incubation in the buffer (red line) and Sb NSs treated with PBS/H_2O_2/hMPO (blue line). (b) f-Sb nanosheets in buffer at 0 h (black line) and after 10 h of incubation in the buffer (red line), and f-Sb nanosheets treated with PBS/H_2O_2 /hMPO for 10 h (blue line).

Open Access Article. Published on 25 marca 2025. Downloaded on 02.02.2026 17:35:17.
This article is licensed under a Creative Commons Attribution-NonCommercial 3.0 Unported Licence.

nanosheets. Importantly, functionalized Sb nanosheets showed less degradation compared to pristine Sb nanosheets, which can be attributed to the increased physiological stability provided by the cyclodextrin coatings.[22] These results suggested that the peroxidase activity of hMPO was responsible for the degradation of the Sb nanosheets.

3.4 Degradation of Sb and f-Sb nanosheets using HRP

The degradation of the nanosheets was also studied using a plant enzyme, HRP. The experiment involved the incubation of both Sb and f-Sb nanosheets in the presence of HRP and H_2O_2, wherein the HRP was renewed every day for 10 days. First, the degradation of the nanosheets was characterized using TEM analyses and the Raman spectroscopic technique to compare the differences in the morphology and structure at 0 and after 10 days. Fig. 5a and b show the TEM images of Sb nanosheets at 0 and 10 days of incubation in PBS, respectively. The results suggested that the nanosheets were quite stable in the buffer at day 0 with distinct edges and boundaries. However, after 10 days, partial degradation was observed with both a sheet-like morphology as well as the visible formation of small pores. Furthermore, Fig. 5c displays the Sb nanosheets at 10 days in the presence of H_2O_2 alone, revealing no significant difference in the morphology of the nanosheet apart from a small amount of debris formation. Furthermore, Fig. 5d shows the Sb nanosheets after treatment with HRP/H_2O_2, where the sheet morphology was completely lost, and there were more debris and porous structures. This concluded that similar to hMPO, HRP also mediated the oxidation or degradation of Sb nanosheets. Furthermore, in the case of the f-Sb nanosheets, the nanosheets incubated in PBS buffer at 0 and 10 days showed no significant difference in the morphology (Fig. 5e and f), indicating the stability of f-Sb nanosheets stabilized with β-CDs. Similarly, when the nanosheets were incubated in H_2O_2 alone (Fig. 5g), the nanosheets were still stable and no degradation was observed. Finally, in the presence of HRP/H_2O_2, the nanosheets showed moderate degradation with a small amount of debris, unlike the pristine Sb sheets (Fig. 5h). This indicated the higher stability of the f-Sb nanosheets compared to the pristine nanosheets; these results are similar to the results obtained for degradation by hMPO.

Raman spectroscopic analyses were carried out to confirm the TEM results. The Raman spectra of Sb and f-Sb nanosheets (Fig. 6a and b, respectively) show characteristic peaks of Sb sheets in PBS buffer at day 0. However, in both cases, Sb and f-Sb nanosheets showed broadening of the peaks and a significant reduction in peak intensity after 10 days of incubation in PBS, which could be due to the aggregation of the nanosheets and the formation of the oxide form of Sb.[29–31] However, a clear difference in the Raman analyses was observed for samples after 10 days of degradation using HRP/H_2O_2. There was a complete disappearance of the characteristic peak of pristine Sb nanosheets, as shown in Fig. 6a, which confirmed the heavy oxidation of Sb nanosheets.[29–31] However, the f-Sb nanosheets (Fig. 6b) showed highly broadened peaks (similar to the f-Sb nanosheets incubated in PBS for 10 hours), confirming that some residual f-Sb nanosheets were still present in the buffer, demonstrating partial degradation of f-Sb nanosheets. This partial degradation could be ascribed to the protective effect of functionalization, which imparts stability.

3.5 Cytotoxicity of Sb and f-Sb nanosheets in THP-1 human monocytes

The cytotoxicity of both pristine and functionalized Sb-nanosheets before and after degradation was observed in THP-1 cells. Fig. 7 shows the cytotoxicity induced by Sb-

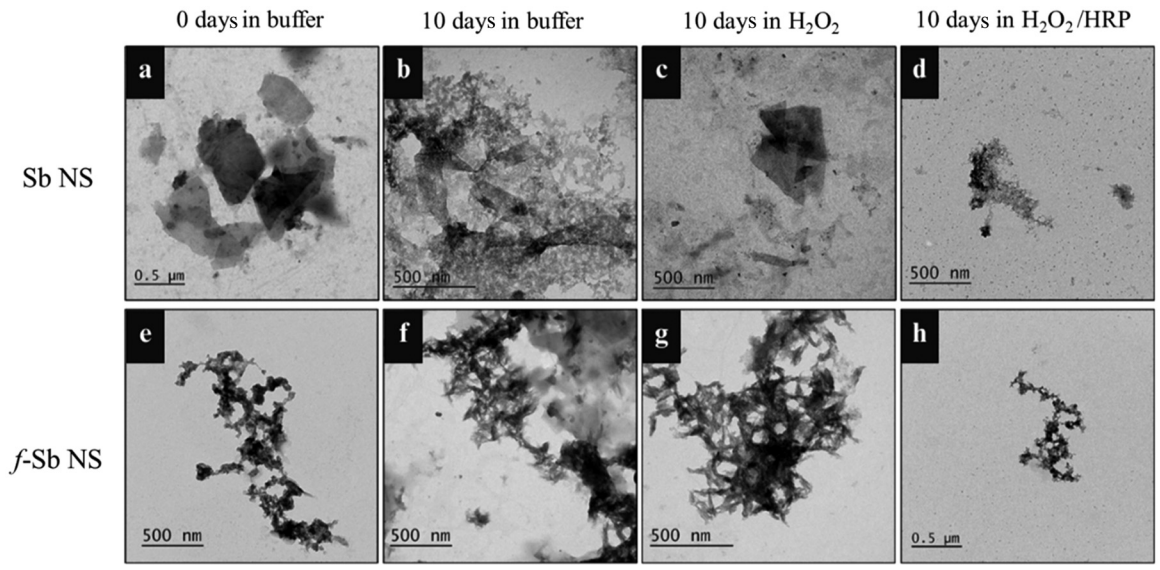

Fig. 5 TEM images of HRP-catalysed degradation of (a) Sb NSs and (e) f-Sb NSs dispersed in buffer on day 0. (b) Sb NSs and (f) f-Sb NSs after 10 days of incubation in the buffer. (c) Sb NSs and (g) f-Sb NSs in the buffer, along with H_2O_2, after 10 days of incubation. (d) 10 day treated Sb NSs and (h) f-Sb NSs with PBS/H_2O_2/HRP.

 This journal is © The Royal Society of Chemistry 2025

Open Access Article. Published on 25 marca 2025. Downloaded on 02.02.2026 17:35:17.
This article is licensed under a Creative Commons Attribution-NonCommercial 3.0 Unported Licence.

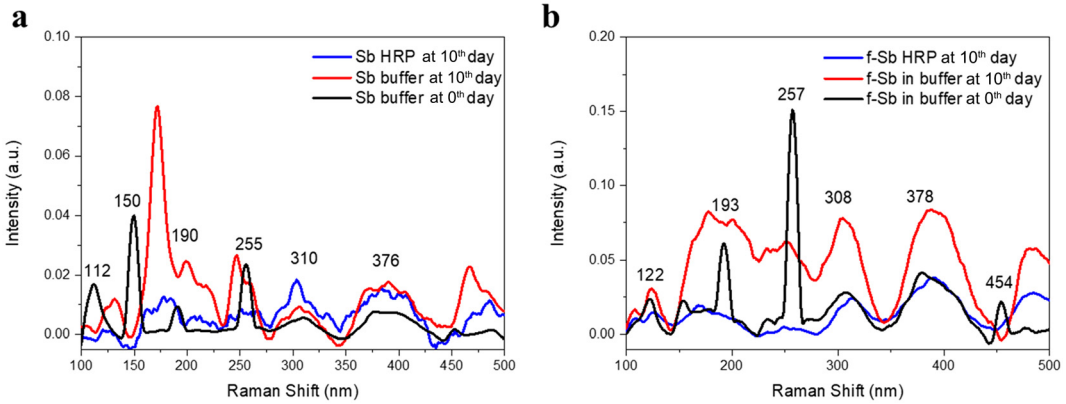

Fig. 6 Raman spectra of (a) Sb NSs dispersed in buffer on day 0 (black line) and after 10 days of incubation in the buffer (red line) and Sb NSs treated with PBS/H_2O_2 /HRP (blue line). (b) f-Sb nanosheets in the buffer on day 0 (black line) and after 10 days of incubation in the buffer (red line), and f-Sb nanosheets after 10 days of treatment with PBS/H_2O_2 /HRP (blue line).

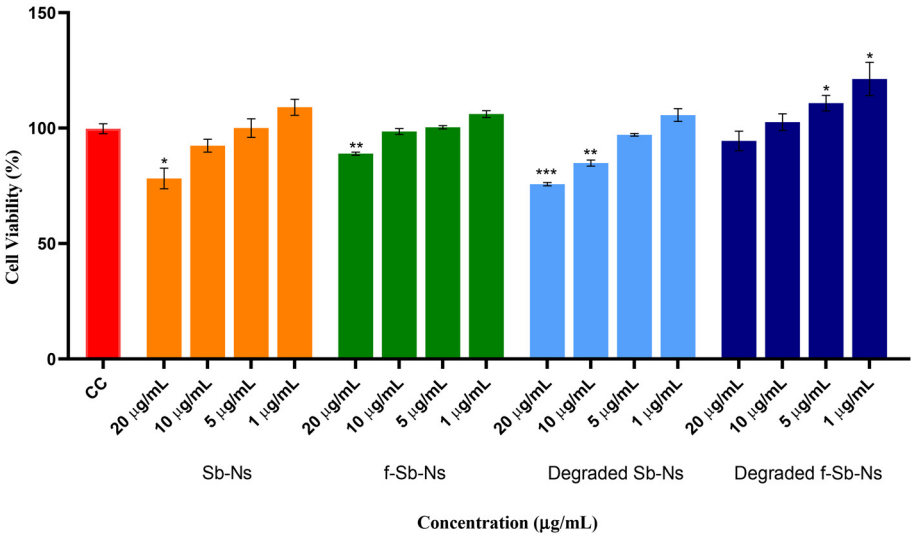

Fig. 7 Cytotoxicity analysis of Sb nanosheets and f-Sb nanosheets done before and after degradation using THP-1 cells. The experiment was performed in triplicate (n = 3); no. of cells: 10 000; incubated with compounds for 24 hours; Sb-nanosheet concentration: 20, 10, 5, and 1 μg mL^{-1}; cell control (CC) containing THP-1 cells only. Statistical comparison is made between the cell control and nanosheets, Student's t-test, unpaired, parametric; *p value ≤0.05; **p value ≤0.01; and ***p value ≤0.001.

nanosheets at higher doses (20 μg mL^{-1} and 10 μg mL^{-1}) compared to the cell control. However, f-Sb-nanosheets showed lower cytotoxicity compared to pristine Sb-nanosheets even at higher concentrations, for both non-degraded and partially degraded Sb and f-Sb nanosheets. The reduced toxicity upon functionalised Sb nanosheets may be due to the cyclodextrin coating.[22] Moreover, partially degraded pristine Sb-nanosheets showed slightly higher cytotoxicity at higher concentrations than the nanosheets before degradation, which could be due to the higher biocompatibility of the oxidation of antimony (Sb).[33] Interestingly, partially degraded f-Sb-nanosheets induced the proliferation of THP-1 cells instead of killing them in comparison with the f-nanosheets before degradation, which might suggest the involvement of processes like degradation-associated maturation.[34]

3.6 Immunomodulatory activity of Sb nanosheets – TNF-α production analysis

TNF-α is a major pro-inflammatory cytokine and regulates various immune responses. It acts as a chemical messenger in the immune system. While various metal nanomaterials have been studied for their immunomodulatory roles, there is limited research on Sb nanosheets. Investigating the immunomodulatory activity of pristine and functionalized Sb nanosheets before and after degradation in human cells would be valuable. Hence, we decided to investigate the effect of Sb-nanosheets in the production of TNF-α. We estimated the amount of TNF-α produced by THP-1 cells upon Sb-nanosheet treatment. As shown in Fig. 8, THP-1 cells alone do not produce any TNF-α. Compared to the cell control, Sb-

Open Access Article. Published on 25 marca 2025. Downloaded on 02.02.2026 17:35:17.
This article is licensed under a Creative Commons Attribution-NonCommercial 3.0 Unported Licence.

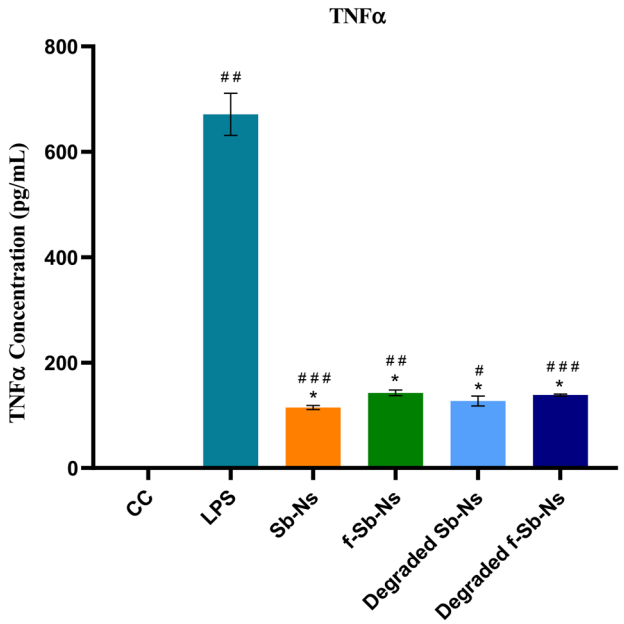

Fig. 8 Immunomodulatory activity of Sb nanosheets assessed through TNF-α production analysis. The experiment was performed with two independent sets in triplicate (n = 6); no. of cells: 20 000; incubated with compounds for 24 hours; Sb-nanosheet concentration taken was 5 μg mL^{-1} and LPS was used as a positive control with a concentration of 100 ng mL^{-1}; cell control (CC) containing THP-1 cells only. Statistical comparison was made between LPS and nanosheets, Student's t-test, unpaired, non-parametric, Mann–Whitney test; *p value ≤0.05; **p value ≤0.01; and ***p value ≤0.001. Moreover, a statistical comparison was carried out between the cell control and nanosheets as well, Student's t-test, parametric, paired t-test; $^{\#}p$ value ≤0.05; $^{\#\#}p$ value ≤0.01; and $^{\#\#\#}p$ value ≤0.001.

nanosheet treatment resulted in a lower amount of TNF-α production, indicating that Sb-nanosheet treatment is slightly immunostimulatory. However, when compared to LPS, which is used as a universal standard for immunomodulation, Sb-nanosheets before and after partial degradation showed significantly lower production of TNF-α, suggesting no role of Sb-nanosheets at the used concentration in the activation of the immune response. Also, we did not observe any significant differences between pristine and functionalized or degraded and non-degraded Sb nanosheets. The lower immunostimulant activity of Sb-nanosheets attained may be due to the damage-associated molecular pattern structure of nanosheets.

4. Conclusions

In summary, we have first fabricated and characterized the main features of Sb and f-Sb nanosheets with the principal aim to study the degradation of both Sb and f-Sb nanosheets by hMPO and HRP. In particular, we focused our attention on the possible effects of oxidation on the nanomaterials. The structural characterization of Sb nanosheets, synthesized *via* sonication-assisted exfoliation in aqueous medium, suggested that only a limited fraction of metallic antimony may resist oxidation, regardless of the presence of β-cyclodextrin (β-CD). However, the significantly higher absolute intensity of the Raman signals observed in exfoliated species in the presence of β-CD could indicate a greater retention of partially unoxidized material. This effect could be due to the ability of β-CD to interact with oxygen atoms formed on the nanosheet surface, replacing water in the passivation process. Such an interaction could contribute to increased solubility and provide partial protection against further oxidative degradation. As for the biodegradation of the nanomaterials, the higher degradability of Sb sheets was found in the case of hMPO treatment over HRP, which is due to the higher redox potential of enzyme intermediates (Compounds I and II with 1.16 and 1.34 V, respectively) and a strong oxidant, HOCl (1.48 V), produced during the peroxidase activity of hMPO.[44] The HRP radical intermediates (Compounds I and II) have a lower oxidation potential of ~0.9 V, due to which the degradation or oxidation of Sb nanosheets was lower compared to hMPO treatment. Furthermore, the results showed that the functionalization and stability of the Sb nanosheets with β-CDs reduced their degradability significantly, which could be due to the surface coating or adsorption of Sb sheets with β-CDs. Moreover, the cell viability results also match the degradation data, wherein f-Sb showed lower cell toxicity than pristine Sb nanosheets, likely attributed to the formation of Sb_2O_3.

Overall, all the results confirm that the Sb sheets could undergo functionalization-dependent biodegradability upon treatment with the human peroxidase enzyme (hMPO), secreted by the primary immune cells, neutrophils. Furthermore, the cell viability studies also suggested that the biodegradation products of Sb sheets did not affect the human cells. These results could be crucial to understanding the *in vivo* fate of Sb sheets and designing biomedical applications such as cancer theranostics.

Data availability

The data supporting this article have been included as part of the ESI.†

Conflicts of interest

There are no confilct of interest to declare.

Acknowledgements

R. K. sincerely thanks the Science and Engineering Research Board (SERB), India, for the start-up research grant (SRG/2022/000291) and the Department of Biotechnology (DBT), India, for the DBT-RLS fellowship (BT/RLF/Re-entry/20/2020). The authors sincerely thank Mr Livin Paul, Mr Kumar Krishna and Prof. K. George Thomas, School of Chemistry, IISER TVM, for their support in Raman analysis. The authors also thank Mr Alex, Mr Pradeep, and Mr Krishna Kumar for their support in

This journal is © The Royal Society of Chemistry 2025

Open Access Article. Published on 25 marca 2025. Downloaded on 02.02.2026 17:35:17.
This article is licensed under a Creative Commons Attribution-NonCommercial 3.0 Unported Licence.

TEM, and XPS analyses. Swetha K. thanks DST for awarding the DST-INSPIRE Fellowship. S. R. B. would like to thank the Director of the Indian Institute of Chemical Technology, Hyderabad, for providing infrastructure, lab space, and support for an institutional research grant (MLP9033). S. R. B. would like to thank the director of the Indian Institute of Chemical Technology, Hyderabad, for providing infrastructure, lab space, and institutional research grant (MLP9033) support. A. P. is a recipient of the ICMR-JRF fellowship of the Department of Health Research, New Delhi, India. The authors thank Dr Rupinder Kaur, Laboratory of Fungal Pathogenesis, Centre for DNA Fingerprinting and Diagnostics, Hyderabad 500039, Telangana, India, for providing THP-1 cells. C. A., M. S. and J. A. acknowledge the Italian Ministry of Enterprises and Made in Italy (MIMIT) - Award/grant Number : Accordo Innovazione MOPAS – Prog. Nr. F/170014/04/X42 – CUP: B69J22003170005 – COR: 9305859 for financial support. C. A. and J. A. also acknowledge the Italian Ministry of Research and University (MUR), PNNR-National Center for Gene Therapy and Drugs based on RNA Technology - SPOKE7 Biocomputing for financial support.

References

1 J. A. Carrasco, P. Congost-Escoin, M. Assebban and G. Abellán, Antimonene: a tuneable post-graphene material for advanced applications in optoelectronics, catalysis, energy and biomedicine, *Chem. Soc. Rev.*, 2023, **52**(4), 1288–1330.

2 R. Bhuvaneswari, V. Nagarajan and R. Chandiramouli, Recent progress on the synthesis, properties and applications of antimonene - A mini-review, *J. Mol. Graphics Modell.*, 2023, **122**, 108473.

3 F. Kuang, T. Hui, Y. Chen, M. Qiu and X. Gao, Post-Graphene 2D Materials: Structures, Properties, and Cancer Therapy Applications, *Adv. Healthcare Mater.*, 2024, **13**(5), 2302604.

4 J. Kaur, M. Singh, C. Dell'Aversana, R. Benedetti, P. Giardina, M. Rossi, M. Valadan, A. Vergara, A. Cutarelli, A. M. I. Montone, L. Altucci, F. Corrado, A. Nebbioso and C. Altucci, Biological interactions of biocompatible and water-dispersed MoS2 nanosheets with bacteria and human cells, *Sci. Rep.*, 2018, **8**(1), 16386.

5 M. Singh, C. Zannella, V. Folliero, R. Di Girolamo, F. Bajardi, A. Chianese, L. Altucci, A. Damasco, M. R. Del Sorbo, C. Imperatore, M. Rossi, M. Valadan, M. Varra, A. Vergara, G. Franci, M. Galdiero and C. Altucci, Combating Actions of Green 2D-Materials on Gram positive and Negative Bacteria and Enveloped Viruses, *Front. Bioeng. Biotechnol.*, 2020, **8**, 569967.

6 P. Ares, S. Pakdel, I. Palacio, W. S. Paz, M. Rassekh, D. Rodríguez-San Miguel, L. Aballe, M. Foerster, N. Ruiz del Árbol, J.Á Martín-Gago, F. Zamora, J. Gómez-Herrero and J. J. Palacios, Few-layer antimonene electrical properties, *Appl. Mater. Today*, 2021, **24**, 101132.

7 M. Bat-Erdene, G. Xu, M. Batmunkh, A. S. R. Bati, J. J. White, M. J. Nine, D. Losic, Y. Chen, Y. Wang, T. Ma and J. G. Shapter, Surface oxidized two-dimensional antimonene nanosheets for electrochemical ammonia synthesis under ambient conditions, *J. Mater. Chem. A*, 2020, **8**(9), 4735–4739.

8 J. Ji, X. Song, J. Liu, Z. Yan, C. Huo, S. Zhang, M. Su, L. Liao, W. Wang, Z. Ni, Y. Hao and H. Zeng, Two-dimensional antimonene single crystals grown by van der Waals epitaxy, *Nat. Commun.*, 2016, **7**(1), 13352.

9 Y. Duo, Y. Huang, W. Liang, R. Yuan, Y. Li, T. Chen and H. Zhang, Ultraeffective Cancer Therapy with an Antimonene-Based X-Ray Radiosensitizer, *Adv. Funct. Mater.*, 2020, **30**(4), 1906010.

10 W. Tao, X. Ji, X. Zhu, L. Li, J. Wang, Y. Zhang, P. E. Saw, W. Li, N. Kong, M. A. Islam, T. Gan, X. Zeng, H. Zhang, M. Mahmoudi, G. J. Tearney and O. C. Farokhzad, Two-Dimensional Antimonene-Based Photonic Nanomedicine for Cancer Theranostics, *Adv. Mater.*, 2018, **30**(38), e1802061.

11 G. Lu, C. Lv, W. Bao, F. Li, F. Zhang, L. Zhang, S. Wang, X. Gao, D. Zhao, W. Wei and H.-y. Xie, Antimonene with two-orders-of-magnitude improved stability for high-performance cancer theranostics, *Chem. Sci.*, 2019, **10**(18), 4847–4853.

12 J. Wu, X. Cai, G. R. Williams, Z. Meng, W. Zou, L. Yao, B. Hu, Y. Chen and Y. Zheng, 2D antimonene-integrated composite nanomedicine for augmented low-temperature photonic tumor hyperthermia by reversing cell thermoresistance, *Bioact. Mater.*, 2022, **10**, 295–305.

13 X. Jin, C. Xu, J. Hu, S. Yao, Z. Hu and B. Wang, A biodegradable multifunctional nanoplatform based on antimonene nanosheets for synergistic cancer phototherapy and dual imaging, *J. Mater. Chem. B*, 2021, **9**(45), 9333–9346.

14 G. Colotti and A. Ilari, Antimony-Based Therapy of Leishmaniases, Molecular and Cellular Rationale, in *Encyclopedia of Metalloproteins*, ed. R. H. Kretsinger, V. N. Uversky and E. A. Permyakov, Springer New York, New York, NY, 2013, pp. 78–86.

15 M. Bat-Erdene, P. Myagmarsereejid, A. S. R. Bati, J. Qin, Y. L. Zhong, J. G. Shapter and M. Batmunkh, Exfoliated 2D Antimonene-Based Structures for Light-Harvesting Photoactive Layer of Highly Stable Solar Cells, *Small Struct.*, 2022, **3**(6), 2200038.

16 A. R. Sureshbabu, R. Kurapati, J. Russier, C. Ménard-Moyon, I. Bartolini, M. Meneghetti, K. Kostarelos and A. Bianco, Degradation-by-design: Surface modification with functional substrates that enhance the enzymatic degradation of carbon nanotubes, *Biomaterials*, 2015, **72**, 20–28.

17 R. Kurapati, C. Backes, C. Ménard-Moyon, J. N. Coleman and A. Bianco, White Graphene undergoes Peroxidase Degradation, *Angew. Chem., Int. Ed.*, 2016, **55**(18), 5506–5511.

18 R. Kurapati, K. Kostarelos, M. Prato and A. Bianco, Biomedical Uses for 2D Materials Beyond Graphene: Current Advances and Challenges Ahead, *Adv. Mater.*, 2016, **28**(29), 6052–6074.

19 R. Kurapati, L. Muzi, A. P. R. de Garibay, J. Russier, D. Voiry, I. A. Vacchi, M. Chhowalla and A. Bianco,

Open Access Article. Published on 25 marca 2025. Downloaded on 02.02.2026 17:35:17.
This article is licensed under a Creative Commons Attribution-NonCommercial 3.0 Unported Licence.

Enzymatic Biodegradability of Pristine and Functionalized Transition Metal Dichalcogenide MoS2 Nanosheets, *Adv. Funct. Mater.*, 2017, **27**, 1605176.

20 R. Kurapati, C. Martìn, V. Palermo, Y. Nishina and A. Bianco, Biodegradation of graphene materials catalyzed by human eosinophil peroxidase, *Faraday Discuss.*, 2021, **227**(0), 189–203.

21 C. Gibaja, M. Assebban, I. Torres, M. Fickert, R. Sanchis-Gual, I. Brotons, W. S. Paz, J. J. Palacios, E. G. Michel, G. Abellán and F. Zamora, Liquid phase exfoliation of antimonene: systematic optimization, characterization and electrocatalytic properties, *J. Mater. Chem. A*, 2019, **7**(39), 22475–22486.

22 W. Zhao, X. Tan, J. Jiang, F. Liu and T. Mu, Highly Efficient, Green, and Scalable β-Cyclodextrin-Assisted Aqueous Exfoliation of Transition-Metal Dichalcogenides: MoS2 and ReS2 Nanoflakes, *Chem. – Asian J.*, 2017, **12**(10), 1052–1056.

23 G. Abellán, P. Ares, S. Wild, E. Nuin, C. Neiss, D. R.-S. Miguel, P. Segovia, C. Gibaja, E. G. Michel, A. Görling, F. Hauke, J. Gómez-Herrero, A. Hirsch and F. Zamora, Noncovalent Functionalization and Charge Transfer in Antimonene, *Angew. Chem., Int. Ed.*, 2017, **56**(46), 14389–14394.

24 F. Zhang, J. He, Y. Xiang, K. Zheng, B. Xue, S. Ye, X. Peng, Y. Hao, J. Lian, P. Zeng, J. Qu and J. Song, Semimetal–Semiconductor Transitions for Monolayer Antimonene Nanosheets and Their Application in Perovskite Solar Cells, *Adv. Mater.*, 2018, **30**(38), 1803244.

25 H. Kouchakzadeh, S. A. Shojaosadati, A. Maghsoudi and E. Vasheghani Farahani, Optimization of PEGylation conditions for BSA nanoparticles using response surface methodology, *AAPS PharmSciTech*, 2010, **11**(3), 1206–1211.

26 G. Liu, F. Zhang, T. Wu, Z. Li, W. Zhang, K. Han, F. Xing, Z. Man, X. Ge and S. Fu, Single- and Dual-Wavelength Passively Mode-Locked Erbium-Doped Fiber Laser Based on Antimonene Saturable Absorber, *IEEE Photonics J.*, 2019, **11**(3), 1–11.

27 M. Mohamed Ismail, J. Vigneshwaran, S. Arunbalaji, D. Mani, M. Arivanandhan, S. P. Jose and R. Jayavel, Antimonene nanosheets with enhanced electrochemical performance for energy storage applications, *Dalton Trans.*, 2020, **49**(39), 13717–13725.

28 Q. Xiao, C.-X. Hu, H.-R. Wu, Y.-Y. Ren, X.-Y. Li, Q.-Q. Yang, G.-H. Dun, Z.-P. Huang, Y. Peng, F. Yan, Q. Wang and H.-L. Zhang, Antimonene-based flexible photodetector, *Nanoscale Horiz.*, 2020, **5**(1), 124–130.

29 S. Wolff, R. Gillen, M. Assebban, G. Abellán and J. Maultzsch, Two-Dimensional Antimony Oxide, *Phys. Rev. Lett.*, 2020, **124**(12), 126101.

30 G. Mestl, P. Ruiz, B. Delmon and H. Knozinger, Sb2O3/Sb2O4 in reducing/oxidizing environments: an in situ Raman spectroscopy study, *J. Phys. Chem.*, 1994, **98**(44), 11276–11282.

31 D. W. Zeng, C. S. Xie, B. L. Zhu and W. L. Song, Characteristics of Sb2O3 nanoparticles synthesized from antimony by vapor condensation method, *Mater. Lett.*, 2004, **58**(3), 312–315.

32 M. J. Nine, L. Yu, A. L. C. Pereira, M. Batmunkh, K. Hassan, A. M. C. Santos, T. T. Tung and D. Losic, Laminated antimonene as an alternative and efficient shielding strategy against X-ray radiation, *Appl. Mater. Today*, 2022, **29**, 101566.

33 M. Agotegaray, M. G. Blanco, A. Campelo, E. García, R. Zysler, V. Massheimer, M. J. De Rosa and V. Lassalle, β-cyclodextrin coating: improving biocompatibility of magnetic nanocomposites for biomedical applications, *J. Mater. Sci.:Mater. Med.*, 2020, **31**(2), 22.

34 J. Huang, W. Fu, Z. Wei and H. Cao, Antimonene quantum dots as bifunctional fluorescent sensors for rapid detection of cation (Fe3+) and anions (CrO42−, Cr2O72−), *APL Mater.*, 2023, **11**(4), 041101.

35 M. Assebban, C. Gibaja, M. Fickert, I. Torres, E. Weinreich, S. Wolff, R. Gillen, J. Maultzsch, M. Varela, S. Tan Jun Rong, K. P. Loh, E. G. Michel, F. Zamora and G. Abellán, Unveiling the oxidation behavior of liquid-phase exfoliated antimony nanosheets, *2D Mater.*, 2020, **7**(2), 025039.

36 C. Gibaja, D. Rodriguez-San-Miguel, P. Ares, J. Gómez-Herrero, M. Varela, R. Gillen, J. Maultzsch, F. Hauke, A. Hirsch, G. Abellán and F. Zamora, Few-Layer Antimonene by Liquid-Phase Exfoliation, *Angew. Chem.*, 2016, **55**(46), 14345–14349.

37 P. Sahoo, R. C. Sahoo and H. S. S. R. Matte, Determination of Hansen Solubility Parameter and In Situ Visualization of Dispersion Stability of Solution-Processed Antimonene, *ACS Appl. Nano Mater.*, 2023, **6**(23), 21957–21966.

38 Z. Zhang, F. Liu, J. Li and B. Wang, Synergistic phototherapy using chitosan-enhanced antimonene nanosheets for effective cancer treatment, *J. Nanopart. Res.*, 2024, **27**(1), 3.

39 S.-K. Zhang, T. Zhang, C.-E. Hu, Y. Cheng and Q.-F. Chen, The effects of oxidation on the electronic, thermal and mechanical properties of antimonene: First-principles study, *Chem. Phys. Lett.*, 2019, **715**, 56–63.

40 P. Congost-Escoin, M. A. Lucherelli, V. Oestreicher, G. García-Lainez, M. Alcaraz, M. Mizrahi, M. Varela, I. Andreu and G. Abellán, Interplay between the oxidation process and cytotoxic effects of antimonene nanomaterials, *Nanoscale*, 2024, **16**(20), 9754–9769.

41 X. Li, A. M. Aldayel and Z. Cui, Aluminum hydroxide nanoparticles show a stronger vaccine adjuvant activity than traditional aluminum hydroxide microparticles, *J. Controlled Release*, 2014, **173**, 148–157.

42 Y. Guo, S. Guo, J. Ren, Y. Zhai, S. Dong and E. Wang, Cyclodextrin Functionalized Graphene Nanosheets with High Supramolecular Recognition Capability: Synthesis and Host–Guest Inclusion for Enhanced Electrochemical Performance, *ACS Nano*, 2010, **4**(7), 4001–4010.

43 B. Ma, C. Martín, R. Kurapati and A. Bianco, Degradation-by-design: how chemical functionalization enhances the biodegradability and safety of 2D materials, *Chem. Soc. Rev.*, 2020, **49**(17), 6224–6247.

44 R. Kurapati, C. Backes, C. Ménard-Moyon, J. N. Coleman and A. Bianco, White Graphene undergoes Peroxidase Degradation, *Angew. Chem.*, 2016, **55**(18), 5506–5511.